
Expensive Multi-Objective Bayesian Optimization Based on Diffusion Models

Bingdong Li¹ Zixiang Di¹ Yongfan Lu¹ Hong Qian¹ Feng Wang² Peng Yang³ Ke Tang³ Aimin Zhou¹

Abstract

Multi-objective Bayesian optimization (MOBO) has shown promising performance on various expensive multi-objective optimization problems (EMOPs). However, effectively modeling complex distributions of the Pareto optimal solutions is difficult with limited function evaluations. Existing Pareto set learning algorithms may exhibit considerable instability in such expensive scenarios, leading to significant deviations between the obtained solution set and the Pareto set (PS). In this paper, we propose a novel Composite Diffusion Model based Pareto Set Learning algorithm, namely CDM-PSL, for expensive MOBO. CDM-PSL includes both unconditional and conditional diffusion model for generating high-quality samples. Besides, we introduce an information entropy based weighting method to balance different objectives of EMOPs. This method is integrated with the guiding strategy, ensuring that all the objectives are appropriately balanced and given due consideration during the optimization process; Extensive experimental results on both synthetic benchmarks and real-world problems demonstrates that our proposed algorithm attains superior performance compared with various state-of-the-art MOBO algorithms.

1. Introduction

Expensive multi-objective optimization problems are commonly seen various fields, such as neural architecture search (Zoph et al., 2018; Lu et al., 2019), antenna structure design (Ding et al., 2019), and clinical drug trials (Yu et al., 2019). Handling EMOPs involves optimizing multiple (often conflicting) objectives simultaneously with the limit number of function evaluations due to time and financial constraints.

To meet these challenges, multi-objective Bayesian opti-

mization (MOBO) (Laumanns & Ocenasek, 2002), an extension of single-objective Bayesian Optimization (BO) (Moćkus, 1975) for expensive multi-objective optimization problems, has emerged as a promising paradigm. BO itself is recognized as an exceedingly effective strategy for global optimization, particularly noted for its success in addressing black-box optimization issues (Jones et al., 1998; Snoek et al., 2012). The core principle of BO involves creating probabilistic surrogate models that closely represent the black-box functions. These models are utilized in conjunction with acquisition functions to seek out globally optimal solutions. MOBO represents a fusion of Bayesian optimization with multi-objective optimization. A widely adopted MOBO approach is the random scalarization technique, which effectively translates a multi-objective optimization problem into several single-objective optimization problems. Another noteworthy strategy in MOBO involves the use of sophisticated acquisition functions, such as the expected hypervolume improvement (EHVI) (Couckuyt et al., 2014) and predictive entropy search (PES) (Hoffman & Ghahramani, 2015). Among them, Pareto set learning (PSL) based methods (e.g. (Lin et al., 2022)) which aims to modeling the Pareto set via machine learning techniques, have shown promising performance.

However, effectively capturing and modeling complex distributions of limited samples is difficult when faced with expensive multi-objective Bayesian optimization problems (EMOBOPs). Existing PSL algorithms may exhibit considerable instability in expensive scenarios. This instability can lead to significant deviations between the obtained solution set and the true Pareto set (PS). In other words, the quality of the resulting solution set is highly influenced by the performance of the PSL model, which is largely limited on EMOBOPs.

Diffusion model (DM), inspired by the natural diffusion of gases, is a kind of popular deep generative models. The characteristics of DMs, including their distribution coverage, stationary training objective, and effortless scalability (Dhariwal & Nichol, 2021a), have empowered them to not only outperform Generative Adversarial Networks (GANs) in image synthesis tasks (Dhariwal & Nichol, 2021a) but also achieve great success in diverse fields such as computer vision (Baranchuk et al., 2021; Yu et al., 2022), natural language processing (Austin et al., 2021a), and waveform

¹East China Normal University ²Wuhan University ³Southern University of Science and Technology. Correspondence to: Feng Wang <fengwang@whu.edu.cn>, Aimin Zhou <amzhou@cs.ecnu.edu.cn>.

signal processing (Leng et al., 2022). These features of DM show promise for its application in Pareto set learning in EMOBOPs.

In this paper, we propose a novel Composite Diffusion Model based Pareto Set Learning algorithm, namely CDM-PSL for expensive MOBO. We introduce the Diffusion Model into Pareto Set Learning, where DM operates by simulating the transition of data from an ordered state to disordered noise. This process progressively learns and reveals the inherent distribution within the data. This methodology is particularly effective in scenarios with limited sample sizes, as it can efficiently extract substantial information from each individual sample, thereby amplifying the learning impact (Yang et al., 2023). This enables the effective modeling of complex distributions of high-quality samples. Building upon this foundation, to generate samples of superior quality, we designed a guided sampling process. This approach ultimately led to the realization of conditional sample generation.

The major contributions of this paper are summarized as follows: 1) We introduce a composite diffusion model based Pareto set learning method for offspring generation for expensive MOBO, which includes both unconditional and conditional sample generation. 2) We devise a guided sampling process to improve the quality of solutions generated by the diffusion model, resulting in a conditional diffusion model; 3) We introduce an information entropy based weighting method to balance the importance of different objectives of multi-objective problems. This method is integrated with the guiding strategy, ensuring that all the objectives are appropriately balanced and given due consideration during the optimization process; 4) We have conducted extensive experiments on both synthetic benchmarks and real-world problems, clearly demonstrating that CDM-PSL obtains superior performance compared with various state-of-the-art MOBO algorithms.

2. Preliminaries

2.1. Expensive Multi-objective Optimization

A multi-objective optimization problem (MOP) can be universally expressed in mathematical terms as follows:

$$\begin{aligned} & \text{minimize } \mathbf{f}(\mathbf{x}) = (f_1(\mathbf{x}), f_2(\mathbf{x}), \dots, f_M(\mathbf{x}))^T \\ & \text{subject to } \mathbf{x} \in \Omega \end{aligned} \quad (1)$$

where $\mathbf{x} = (x_1, x_2, \dots, x_d)$ represents the decision vector, $\mathbf{f}(\cdot): \Omega \rightarrow \Lambda$ denotes a black-box objective function, encompassing M ($M \geq 2$) objectives, Ω symbolizes the non-empty *decision space*, and Λ is the *objective space*. An MOP is considered expensive when the evaluation of $\mathbf{f}(\mathbf{x})$ involves either time-intensive computations or high-cost experimental procedures. In such contexts, the primary aim in

optimizing an MOP is to approximate the Pareto Front (PF) effectively within a limited evaluation budget.

Definition 2.1 (Pareto dominance). Considering two solutions \mathbf{x} and $\mathbf{y} \in \Omega$, \mathbf{x} is said to *dominate* \mathbf{y} (expressed as $\mathbf{x} \prec \mathbf{y}$) if and only if the following conditions are met: 1) $\forall i \in \{1, 2, \dots, M\}, f_i(\mathbf{x}) \leq f_i(\mathbf{y})$; 2) $\exists j \in \{1, 2, \dots, M\}, f_j(\mathbf{x}) < f_j(\mathbf{y})$. This definition encapsulates the essential criterion for determining the quality of solutions in terms of meeting multiple objectives simultaneously. (Yu, 1974)

Definition 2.2 (Pareto optimal). A solution $\mathbf{x}^* \in \Omega$ is Pareto optimal if there exists no other solution $\mathbf{x} \in \Omega$ that can dominate it. This implies that within the feasible region Ω , \mathbf{x}^* is considered to be Pareto optimal if no alternative solution offers better outcomes across all objectives without being worse in at least one of them.

Definition 2.3 (Pareto Set and Pareto Front). The *Pareto Set* (PS) refers to the collection of all the Pareto optimal solutions: $PS = \{\mathbf{x} \in \Omega | \forall \mathbf{y} \in \Omega, \mathbf{y} \not\prec \mathbf{x}\}$. The corresponding set of objective vectors of the PS is the *Pareto Front* (PF).

2.2. Bayesian Optimization

Bayesian Optimization (BO) is a powerful method for the efficient global optimization of expensive black-box functions (Jones et al., 1998; Shahriari et al., 2015). By leveraging probabilistic surrogate models to approximate the black-box functions, in conjunction with acquisition functions, it seeks to locate global optimal solutions with as few evaluations of the actual objective function as possible. BO has been widely used in a variety of fields, including hyperparameter tuning (Bergstra et al., 2011), A/B testing (Letham et al., 2019), combinatorial optimization (Zhang et al., 2015), among others.

2.3. Diffusion Models

Diffusion models are a specialized form of probabilistic generative models that operate by learning to reverse a forward process that gradually increases noise in the training data (Sohl-Dickstein et al., 2015; Ho et al., 2020). They have demonstrated remarkable performance on a wide variety of tasks, such as image generation (Austin et al., 2021b; Bao et al., 2022), voice synthesis (Liu et al., 2022), video generation (Ho et al., 2022) and inpainting (Lugmayr et al., 2022). Training a diffusion model involves two processes: the forward diffusion process and the backward denoising process.

2.3.1. FORWARD PROCESS

In the forward phase, Gaussian noise is added to the input data step by step until a pure Gaussian noise is produced, which is a Markovian process. Given an initial data distribution $\mathbf{x}_0 \sim q(\mathbf{x})$, the noised x_1, x_2, \dots, x_T can be obtained

from the following equation:

$$q(x_t|x_{t-1}) = \mathcal{N}\left(x_t; \sqrt{1 - \beta_t} \cdot x_{t-1}, \beta_t \cdot \mathbf{I}\right), \forall t \in \{1, \dots, T\},$$

where T is the number of diffusion steps and the step sizes are controlled by a variance schedule $\{\beta_t \in (0, 1)\}_{t=1}^T$. Moreover, the properties of this recursive formula make it possible to obtain $q(x_t)$ directly from x_0 by the following equation:

$$q(x_t|x_0) = \mathcal{N}\left(x_t; \sqrt{\hat{\beta}_t} \cdot x_0, (1 - \hat{\beta}_t) \cdot \mathbf{I}\right), \forall t \in \{1, \dots, T\},$$

where $\hat{\beta}_t = \prod_{i=1}^t \alpha_i$ and $\alpha_t = 1 - \beta_t$. Thus, x_t can be sampled from $q(x_t|x_0)$ as follows:

$$x_t = \sqrt{\hat{\beta}_t} \cdot x_0 + \sqrt{1 - \hat{\beta}_t} \cdot z_t,$$

where $z_t \sim \mathcal{N}(0, \mathbf{I})$.

2.3.2. REVERSE PROCESS

The reverse process recreates the true sample from a Gaussian noise input $x_T \sim \mathcal{N}(0, \mathbf{I})$ by the following equation:

$$q(x_{t-1}|x_t) = \mathcal{N}(x_{t-1}; \mu(x_t, t), \Sigma(x_t, t))$$

However, $q(x_{t-1}|x_t)$ cannot easily be evaluated due to the reverse process lacking a complete dataset and therefore we need to train a neural network $p_\theta(x_{t-1}|x_t) = \mathcal{N}(x_{t-1}; \mu_\theta(x_t, t), \Sigma_\theta(x_t, t))$ to approximate these conditional probabilities. Specifically, The model takes in the noisy data x_t and the corresponding embedding at time step t as input, and is trained to predict the mean $\mu_\theta(x_t, t)$ and the covariance $\Sigma_\theta(x_t, t)$. Based on this, Ho (Ho et al., 2020) proposed to fix the covariance $\Sigma_\theta(x_t, t)$ to a constant value and reformulating the mean $\mu_\theta(x_t, t)$ as a function dependent on noise, as follows:

$$\mu_\theta = \frac{1}{\sqrt{\alpha_t}} \cdot \left(x_t - \frac{1 - \alpha_t}{\sqrt{1 - \hat{\beta}_t}} \cdot z_\theta(x_t, t) \right).$$

This enables the model to predict the noise of the data rather than directly predicting the mean and the covariance.

2.4. Conditional Generative Models

In the field of generative models, Conditional Generative Models have garnered significant interest (Odena et al., 2017; Gong et al., 2019). A prominent approach in Generative Adversarial Networks (GANs) involves incorporating a classification component within the Discriminator network. The strategy aims to facilitate the learning of classifier conditions, a method explored in various studies (Zhao et al., 2020; Kang et al., 2021; Dung & Binh, 2022). The training

of these classifiers proceeds concurrently with the GAN training process.

Similarly, Deep Generative Models (DGMs) have been adapted to include conditional capabilities. This is achieved by integrating a classification head into diffusion models, as demonstrated in recent work (Song et al., 2020). There are instances where DGMs are conditioned on images, enabling style transfer across different instances, a concept explored by Preechakul (Preechakul et al., 2022). The research by Dhariwal and Nichol (Dhariwal & Nichol, 2021b) presents a novel method allowing for the control of samplers/generators in DGMs without necessitating retraining. This idea is further expanded by Liu et al. (Liu et al., 2023), who generalize this concept to accommodate various modalities. In the realm of guidance without classifiers, Ho and Salimans (Ho & Salimans, 2022) have shown that it's possible to achieve guidance properties in generative models without relying on a classifier.

2.5. Diffusion Model Based Optimization Algorithms

Krishnamoorthy proposed a black-box optimization algorithm named DDM (Krishnamoorthy et al., 2023), based on the diffusion model. This algorithm converts a single-objective optimization problem into a continuous diffusion process, leveraging the inverse process of the diffusion model to efficiently address complex problems. Subsequently, Yan and Jin's EmoDM (Yan & Jin, 2024) extended the application of the diffusion model to multi-objective optimization. By learning the noise distribution in the previous evolutionary search task, a set of non-dominated solutions can be generated for the new multi-objective optimization problem without further evolutionary search. Fang's DMO (Fang et al., 2024) further demonstrates the diffusion model's efficacy by applying it to create a gasoline hybrid scheduling scheme, highlighting its capability in solving practical multi-objective optimization challenges. Building upon these contributions, this paper's CDM-PSL advances the field by optimizing the balance between solution convergence and diversity through the integration of conditional and unconditional diffusion models. Moreover, CDM-PSL incorporates gradient information, weighted by information entropy, into the process of generating solutions, significantly enhancing convergence performance during the early-stage iterations. The combination of these strategies makes CDM-PSL have competitive performance in solving expensive multi-objective Bayesian optimization problem.

3. Our Method

3.1. Overview

We present a composite diffusion model based Pareto set learning method for EMOBO, denoted as CDM-PSL (AI-

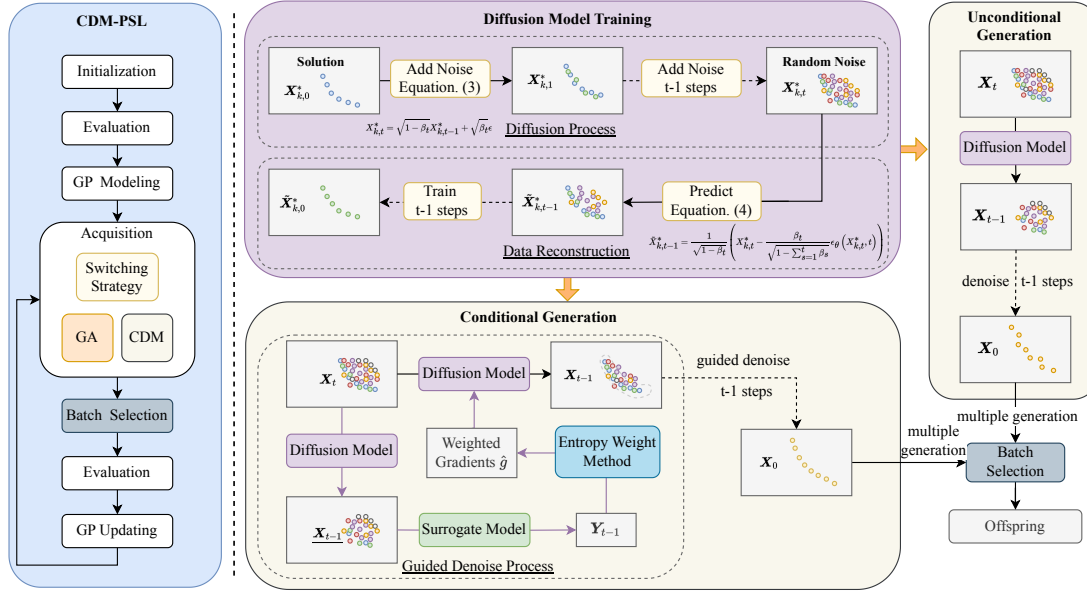


Figure 1. (left) The framework of CDM-PSL. (right) Diffusion Model Training (DMT), Conditional Generation (CG), and Unconditional Generation (UG). DMT involves learning from the selected samples through multiple steps; CG is designed to create high-quality samples with an optimized distribution; UG is used to generate diverse samples with high efficiency.

gorithm 1 and Figure 1). CDM-PSL contains three components to generate offspring: data extraction, diffusion model training and conditional generation. Initially, the process begins by initializing a set of samples $X_0 \subset \mathcal{X}$, where $\mathcal{X} \subset \mathcal{R}^d$. These samples are drawn using *Latin Hypercube Sampling* (LHS) (McKay et al., 2000). Following this initialization, acquisition and batch selection are then applied in an iterative manner.

3.2. Data Extraction

To prepare training data for Pareto set learning, we propose a data extraction strategy summarized in Algorithm 2. Central to this strategy is the application of shift-based density estimation (SDE) (Li et al., 2013) for calculating fitness values, which is mathematically represented as:

$$Fitness(\mathbf{p}) = \min_{\mathbf{q} \in Y_k \setminus \mathbf{p}} \sqrt{\sum_{i=1}^M (\max\{0, f_i(\mathbf{q}) - f_i(\mathbf{p})\})^2} \quad (2)$$

In this formula, \mathbf{p} and \mathbf{q} are solutions within the set Y_k , and $f_i(\mathbf{p})$ indicates the i -th objective value of solution \mathbf{p} . The SDE methodology assesses the quality of samples based on their convergence and diversity characteristics. From X_k , a total of T candidate solutions (for instance, $\lfloor \frac{|X_k|}{3} \rfloor$) that demonstrate superior SDE values are identified as Pareto optimal samples. This selection process is essential for ensuring the quality and relevance of the data used in Pareto set learning.

3.3. Diffusion Model Training

The DM training process comprises two major steps: the diffusion process and noise prediction.

3.3.1. DIFFUSION PROCESS

Given set of samples X_k^* and a specified step t , the diffusion process involves gradually introducing Gaussian noise $\epsilon \sim \mathcal{N}(0, I)$ to X_k^* over t steps:

$$X_{k,t}^* = \sqrt{1 - \beta_t} X_{k,t-1}^* + \sqrt{\beta_t} \epsilon \quad (3)$$

In this equation, $X_{k,t}^*$ denotes the data at step t , and $\beta_t \in [1e-5, 5e-2]$ represents the noise level at step t . The DM learning process for PSL operates as a Markov chain. This stepwise approach simplifies the learning task compared to direct Pareto set learning and effectively captures the distribution characteristics of optimal samples.

3.3.2. NOISE PREDICTION

The noise prediction phase involves reconstructing the samples $X_{k,t}^*$, which have undergone the diffusion process, back to their original state, X_k^* . This reconstruction is achieved through a model \mathcal{M} that predicts the noise added at each step, thereby reversing the diffusion process. This process

Algorithm 1 The framework of MOBO with CDM-PSL

Input: black-box function $f(x)$, number of iterations K , batch size B , number of initial solutions N
Output: final solutions $\{X_K, Y_K\}$, Pareto front \mathcal{P}_f
 Initialize N solutions $\{X_0, Y_0\}$ by LHS
for $k = 0$ **to** $K - 1$ **do**
 Train surrogate model GP_i^k based on $\{X_k, Y_k\}$ for each objective $f_i, i = 1, \dots, M$
 $X_k^* \leftarrow$ Data extraction based on $\{X_k, Y_k\}$ (**Algorithm 2**)
 if F_{CDM} is True **then**
 $S \leftarrow$ Pareto set learning based on X_k^* by CDM-PSL (**Algorithm 3**)
 else
 $S \leftarrow$ Generate offspring using *Optimizer*
 end if
 $X_k^B \leftarrow$ Batch selection based on GP^k, S and $\{X_k, Y_k\}$
 Evaluate and update $X_{k+1} \leftarrow X_k \cup X_k^B, Y_{k+1} \leftarrow Y_k \cup f(X_k^B)$
 Decide whether to invert F_{CDM} based on HV
end for
 Approximate the Pareto front \mathcal{P}_f by non-dominated solutions in Y_K

Algorithm 2 Data Extraction

Input: all already-evaluated solutions in the k -th iteration $\{X_k, Y_k\}$, number of real samples T
Output: solutions after data extraction X_k^*
Fitness \leftarrow Calculate the fitness of each solution in $\{X_k, Y_k\}$ by Eq. 2
 $X_k^* \leftarrow$ Select top T candidate solutions with *Fitness*

follows the equation 4:

$$\tilde{X}_{k,t-1}^* = \frac{1}{\sqrt{1-\beta_t}} \left(X_{k,t}^* - \frac{\beta_t}{\sqrt{1-\sum_{s=1}^t \beta_s}} \epsilon_\theta(X_{k,t}^*, t) \right). \quad (4)$$

In this equation, $\tilde{X}_{k,t-1}^*$ represents the data after reconstruction, and θ denotes the parameters of the model. The term $\epsilon_\theta(X_{k,t}^*, t)$ is the predicted noise by model \mathcal{M} at step t . The loss function \mathcal{L} for model \mathcal{M} is defined as:

$$\mathcal{L} = \frac{1}{\mathcal{H}} \sum_{i=1}^{\mathcal{H}} (\epsilon - \epsilon_\theta(x_{k,i,t}^*, t)). \quad (5)$$

This equation takes \mathcal{H} into account, the total number of optimal samples, where each $x_{k,i,t}^*$ is an instance from $X_{k,t}^*$, and $\epsilon_\theta(X_{k,t}^*, t)$ represents the predicted noise. The training of \mathcal{M} , using Equation 5, aims to minimize the loss \mathcal{L} , thereby enhancing the accuracy of noise prediction. The entire DM training process, comprising both the diffusion process and noise prediction, plays a crucial role in

Algorithm 3 Composite Diffusion Model based Generation

Input: trained model \mathcal{M}
Parameter: steps T , number of generation N_1, N_2
Output: solutions generated by CDM S
 $S \leftarrow \emptyset$
for $i = 1$ **to** N_1 **do**
 for $t = T$ **to** 1 **do**
 $z \sim \mathcal{N}(\mathbf{0}, \mathbf{I})$
 $\hat{g} \leftarrow$ Calculate weighted gradient by entropy weight method and surrogate model
 $x_{t-1} \leftarrow \frac{1}{\sqrt{\alpha_t}} \left(x_t - \frac{1-\alpha_t}{\sqrt{1-\alpha_t}} \epsilon_\theta(x_t, t) \right) + \sigma_t^2 \hat{g} + \sigma_t z$
 end for
 $S \leftarrow S \cup \{x_0\}$
end for
for $i = 1$ **to** N_2 **do**
 for $t = T$ **to** 1 **do**
 $z \sim \mathcal{N}(\mathbf{0}, \mathbf{I})$
 $x_{t-1} \leftarrow \frac{1}{\sqrt{\alpha_t}} \left(x_t - \frac{1-\alpha_t}{\sqrt{1-\alpha_t}} \epsilon_\theta(x_t, t) \right) + \sigma_t z$
 end for
 $S \leftarrow S \cup \{x_0\}$
end for

effective Pareto Set Learning for EMOBOPs. This method presents a novel approach to learning high-quality solutions, striking a balancing between exploration and exploitation in the search space.

3.4. Conditional Generation

In order to further enhancing the quality of generated samples, we propose a Guided Denoise Process. This process leverages gradients to guide the denoising procedure of DM, thereby achieving the realization of a Conditional Diffusion Model. The subsequent elucidation will provide a detailed explanation through two components: the guided denoise process and the weighted gradient.

3.4.1. GUIDED DENOISE PROCESS

For a given step t and sample x_t , the denoising process with guidance can be implemented through equation 6:

$$X_{t-1} = \frac{1}{\sqrt{\alpha_t}} \left(X_t - \frac{1-\alpha_t}{\sqrt{1-\alpha_t}} \epsilon_\theta(X_t, t) \right) + \sigma_t^2 \hat{g} + \sigma_t z \quad (6)$$

where α_t represents $1 - \beta_t$, $\epsilon_\theta(X_t, t)$ signifies the predicted noise by the trained model, σ_t is the standard deviation of the t -th step, and \hat{g} denotes the weighted gradients used to guide the denoising process.

To procure the gradients essential for guiding the model in sample generation, we establish separate Gaussian Process (GP) models for each objective, as proposed by Balandat (Balandat et al., 2020). These models are utilized to compute the objective values for all generated samples, thus obtaining

gradients g for each objective, facilitating the realization of conditional generation.

3.4.2. WEIGHTED GRADIENTS

In addressing EMOPs, employing weighted gradients is essential. This requires the determination of appropriate weights for each objective. Therefore, we propose a weighting methodology grounded in information entropy, facilitating the derivation of these weighted gradients \hat{g} .

In order to obtain weights based on information entropy, it is necessary to first normalize the objective values. Let y_{ij} represent the j -th objective value of the i -th individual. The normalized objective value \tilde{y}_{ij} is computed using Equation 7 as follows:

$$\tilde{y}_{ij} = \frac{y_{ij} - \min(y_j)}{\max(y_j) - \min(y_j)} \quad (7)$$

Subsequent to this, for each objective $j(j = 1, 2, \dots, M)$, the probability matrix P_{ij} is calculated using Equation 8, where $k = 1, 2, \dots, N$ and N represents the number of individuals in the population.

$$P_{ij} = \frac{\tilde{y}_{ij}}{\sum_{k=1}^N \tilde{y}_{kj}} \quad (8)$$

Subsequently, for each objective $j(j = 1, 2, \dots, M)$, the information entropy E_j is computed. The method of calculation is as outlined in Equation 9:

$$E_j = -\frac{1}{\ln(N)} \sum_{i=1}^N (P_{ij} \times \ln(P_{ij} + \eta)) \quad (9)$$

Herein, $i = 1, 2, \dots, N$ and $j = 1, 2, \dots, M$, where N signifies the total number of samples, and M represents the quantity of objectives. To avoid the occurrence of $\ln(0)$, a small positive number, η , is introduced. The computation of information entropy relies on Shannon entropy (Shannon, 1948), expressed as $H(X) = -\sum (P(x) \times \log(P(x)))$. Additionally, the coefficient $\frac{1}{\ln(N)}$ is employed to guarantee that the values of information entropy are confined within the range of 0 to 1.

Finally, for each objective $j = 1, 2, \dots, M$, the weight W_j is computed using Equation 10, where $k = 1, 2, \dots, M$, and M denotes the total number of objectives.

$$W_j = \frac{1 - E_j}{\sum_{k=1}^M (1 - E_k)} \quad (10)$$

By employing the calculated weights W , we can subsequently derive the entropy weighted gradients (EWG) \hat{g} . The entropy weighting method, serving as an adaptive weight allocation approach, assigns weights based on the information entropy of objectives. This method reduces

subjectivity in weighting gradients for different objective values, and ensures that the algorithm places more emphasis on objectives with rich information content, thereby achieving better performance in multi-objective optimization problems. Furthermore, the characteristic of weight allocation based on information entropy endows the entropy weighting method with broad applicability, making it suitable for a wide range of fields and various types of multi-objective optimization problems, demonstrating its strong universality. In the context of guiding the denoising process, the weighted gradients also enhance the effectiveness of the guidance for multi-objective problems, thereby enhancing the conditional generation.

3.5. Selection Strategy

3.5.1. BATCH SELECTION

After obtain the solutions sampled by the CDM-PSL, we employ the batch selection strategy of PSL-MOBO (Lin et al., 2022) to select a small subset $X_k^B = \{x_b | b = 1, \dots, B\}$. Specifically, this strategy use the Hypervolume (HV) indicator (Zitzler & Thiele, 1999) as the selection criteria. The HV indicator is defined as follows:

$$\mathbf{HV}(S) = \Lambda(\{q \in \mathbb{R}^d | \exists p \in S : p \leq q \text{ and } q \leq r\}) \quad (11)$$

where S signifies a solution set, r is identified as a reference vector set, and $\Lambda(\cdot)$ denotes the Lebesgue measure.

3.5.2. OPERATOR SELECTION

At the end of each iteration round, we have devised a method to switch operators based on the growth rate of the HV indicator. In algorithm 1, F_{CDM} is a flag used to determine if CDM is currently being used to generate offspring. After passing through an iteration window, such as three evaluation rounds, if the HV indicator's growth rate falls below a predefined threshold (default setting is 5%), we switch the operator for offspring generation (including CDM-PSL and other *Optimizer* like the Genetic Algorithm (GA)). This strategy is designed to prevent the algorithm from becoming trapped in local optima specific to the current operator.

4. Experiments Study

4.1. Experimental Settings

Instances and Baselines To comprehensively validate the performance of CDM-PSL, experiments were conducted on 9 benchmark problems (2- and 3-objective ZDT1-3 (Zitzler et al., 2000) and DTLZ2-7 (Deb et al., 2005)) and 7 real-world problems (Tanabe & Ishibuchi, 2020).

Moreover, we have compared CDM-PSL with 9 state-of-the-art and classical algorithms, including NSGA-II (Deb et al., 2002), MOEA/D-EGO (Zhang et al., 2009), TSEMO

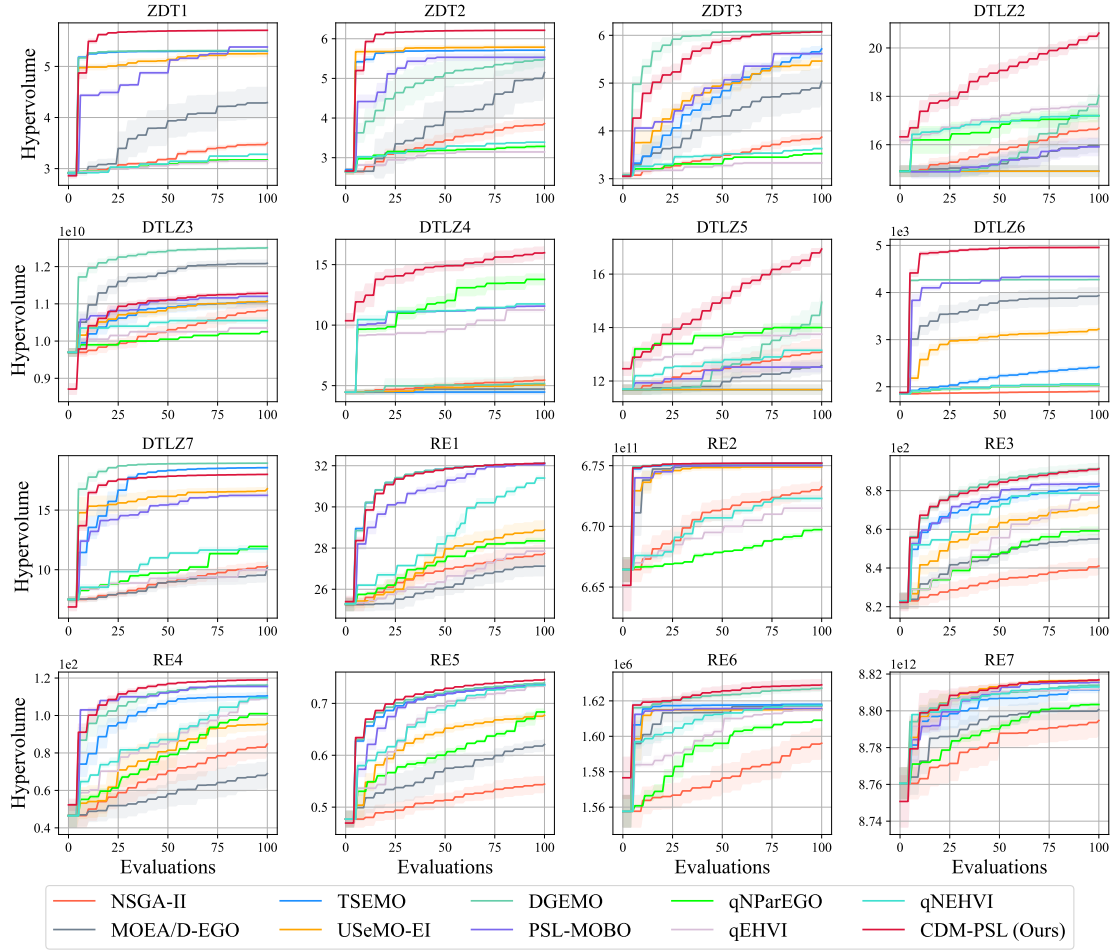


Figure 2. The HV results of 10 algorithms, evaluated on synthetic test functions and real-world problems ($d = 20$). The horizontal axis denotes the FEs after the initialization phase, similarly hereinafter.

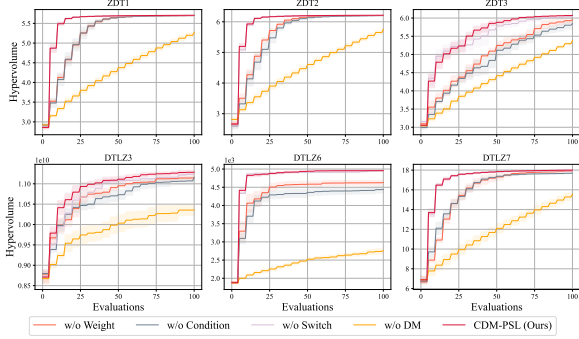


Figure 3. Ablation results of CDM-PSL on 6 instances.

(Bradford et al., 2018), USeMO-EI (Belakaria et al., 2020), DGEMO (Konakovic Lukovic et al., 2020), PSL-MOBO (Lin et al., 2022), qNparEGO (Knowles, 2006), qEHVI (Daulton et al., 2020) and qNEHVI (Daulton et al., 2021).

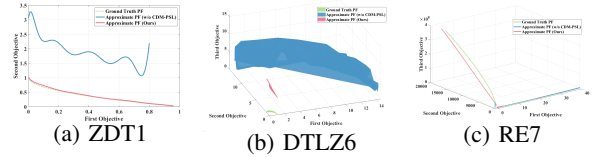


Figure 4. Approximate Pareto fronts obtained by CDM-PSL and MOBO w/o CDM-PSL.

Instances and Parameter Settings For fair comparison, the population size N was initialized to 100 for all the compared algorithms. Bayesian optimization algorithms were executed for 20 batches, each with a batch size of 5, across all algorithms. Each method was randomly run 10 times. For CDM-PSL, the hyperparameter t was set to 25, the batch size m was 1024, and the learning rate γ was 0.001, with training spanning 4000 epochs. The configurations for other methods were aligned with those in their original publications (See the appendix).

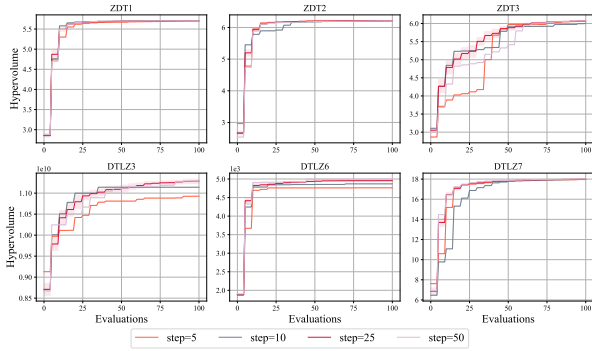


Figure 5. The HV values relative to the number of FEs for CDM-PSL with different number of steps t .

Evaluation Metrics The hypervolume (HV) indicator, as defined in Equation 11, was employed to assess the quality of the solutions obtained. Higher HV values are indicative of better performance.

4.2. Experimental Results

We conducted a series of experiments on a variety of widely recognized synthetic multi-objective benchmarks, including ZDT1-3 (Zitzler et al., 2000) and DTLZ2-7 (Deb et al., 2005). The problems selected for the experiments featured 2 and 3 objectives, with the number of decision variables set at 20. We particularly highlight the results for a specific instance where $d = 20$, and further details are available in the supplementary materials. Additionally, the comprehensive performance of CDM-PSL was thoroughly evaluated through the application of seven real-world problems.

Figure 2 shows a comparison of the hypervolume (HV) indicator relative to function evaluations (FE). CDM-PSL demonstrates outstanding performance across most synthetic benchmarks, excelling in both convergence speed and final values. Additionally, CDM-PSL exhibits ideal performance in real-world problems (RE). These findings decisively affirm the effectiveness and superiority of the CDM-PSL approach.

4.3. Ablation Study

To verify the effectiveness of each component in CDM-PSL, ablation study results are presented in Figure 3.

Entropy Weight CDM-PSL w/o Weight represents the CDM-PSL variant using mean weighted gradients to guide the sampling process instead of entropy weighted gradients (EWG). CDM-PSL demonstrates superior convergence performance compared to CDM-PSL w/o Weight on all the six tested problems and attains better final values in ZDT3, DTLZ3 and DTLZ6. This indicates that EWG can gauge the

significance of objectives more accurately, thereby offering more effective guidance for the sampling process.

Conditional Generation CDM-PSL w/o Condition refers to the variant from which the conditional generation component has been omitted. In a similar vein, CDM-PSL consistently and significantly outperforms CDM-PSL w/o Condition across all the tested problems. This clearly validates the critical role and effectiveness of the conditional generation component in the CDM-PSL.

Switching Strategy CDM-PSL w/o Switch is a variation of CDM-PSL that lacks the switching strategy. The results of the ablation experiments on ZDT3 and DTLZ3 demonstrate that the inclusion of this strategy prevents the PSL model from falling into local optima, achieved through alternating between various optimization operators. The incorporation of the switching strategy in CDM-PSL results in enhanced convergence performance.

Diffusion Model CDM-PSL w/o DM refers to the variant that employs the Genetic Algorithm (GA) instead of the DM-based PSL model as its optimizer, utilizing Simulated Binary Crossover (SBX) to generate new solutions. It is evident that this version’s performance is markedly inferior compared to that of the standard CDM-PSL. This disparity underscores the effectiveness of DM based Pareto set learning.

4.4. Validity of CDM-PSL

Figure 4 displays the Pareto fronts approximated by CDM-PSL and by MOBO without CDM-PSL, based on the posterior mean. Clearly, CDM-PSL more effectively captures the essential features of the true PF, surpassing MOBO without CDM-PSL, in both synthetic benchmarks and real-world problems. For instance, MOBO without CDM-PSL is difficult to approach the true PF in a limited number of evaluations, yet CDM-PSL can effectively capture nearly all characteristics of ZDT1. In the three-objective DTLZ6 problem, the use of CDM-PSL can approximate the true PF faster in a limited number of evaluations. Additionally, our methodology demonstrates commendable exploitation capabilities on complex problems, such as the rocket injector design (RE7) (Vaidyanathan et al., 2003), which is characterized by a complex PF. This complexity arises from Pareto optimal solutions being distributed across multiple regions.

4.5. Parameter Sensitivity Study

The main parameter of CDM-PSL, step t , is studied in this subsection. Figure 5 depicts the influence of varying t values on CDM-PSL’s performance. The default value of t is set at 25 in CDM-PSL. A smaller t yields suboptimal experimental outcomes; although near-excellent final values

can be achieved on certain problems, there is a noticeable decline in convergence performance, attributed to the inadequate learning of the distribution of superior solutions. On the other hand, a larger t , such as 50, results in less stable convergence performance compared to $t = 25$, primarily due to an increase in learning error. Furthermore, an increased step t also leads to longer training durations. Consequently, balancing between convergence performance and time efficiency, $t = 25$ is established as the optimal default step size for CDM-PSL.

5. Conclusion and Future work

In this paper, we introduce a composite diffusion model based Pareto set learning method, termed CDM-PSL, for addressing EMOBOPs. CDM-PSL uses both unconditional and conditional diffusion model for generating high-quality samples. Besides, the quality of the solutions generated by the Pareto Set learning model is significantly enhanced by employing entropy weighted gradients to guide the sampling process. Extensive experimental evaluations on 9 benchmark problems and 7 real-world problems verify the efficiency of CDM-PSL. The relatively high computational overhead makes CDM-PSL challenging to apply in very high-dimensional problems. The Monte Carlo tree approach has proven effective in feature extraction for such complex scenarios (Song et al., 2022). Consequently, there is an intention to incorporate Monte Carlo trees into existing algorithms for future research to address higher-dimensional multi-objective Bayesian optimization problems.

Impact Statements

This paper presents work whose goal is to advance the field of Multi-Objective Bayesian Optimization (MOBO). There are many potential societal consequences of our work, none which we feel must be specifically highlighted here.

References

- Ament, S., Daulton, S., Eriksson, D., Balandat, M., and Bakshy, E. Unexpected improvements to expected improvement for bayesian optimization. *Advances in Neural Information Processing Systems*, 36, 2024.
- Amir, H. M. and Hasegawa, T. Nonlinear mixed-discrete structural optimization. *Journal of Structural Engineering*, 115(3):626–646, 1989.
- Austin, J., Johnson, D. D., Ho, J., Tarlow, D., and Van Den Berg, R. Structured denoising diffusion models in discrete state-spaces. *Advances in Neural Information Processing Systems*, 34:17981–17993, 2021a.
- Austin, J., Johnson, D. D., Ho, J., Tarlow, D., and Van Den Berg, R. Structured denoising diffusion models in discrete state-spaces. *Advances in Neural Information Processing Systems*, 34:17981–17993, 2021b.
- Balandat, M., Karrer, B., Jiang, D., Daulton, S., Letham, B., Wilson, A. G., and Bakshy, E. Botorch: A framework for efficient monte-carlo bayesian optimization. *Advances in neural information processing systems*, 33:21524–21538, 2020.
- Bao, F., Li, C., Zhu, J., and Zhang, B. Analytic-dpm: an analytic estimate of the optimal reverse variance in diffusion probabilistic models. *arXiv preprint arXiv:2201.06503*, 2022.
- Baranchuk, D., Rubachev, I., Voynov, A., Khrukov, V., and Babenko, A. Label-efficient semantic segmentation with diffusion models. *arXiv preprint arXiv:2112.03126*, 2021.
- Belakaria, S., Deshwal, A., Jayakodi, N. K., and Doppa, J. R. Uncertainty-aware search framework for multi-objective bayesian optimization. In *Proceedings of the AAAI Conference on Artificial Intelligence*, volume 34, pp. 10044–10052, 2020.
- Bergstra, J., Bardenet, R., Bengio, Y., and Kégl, B. Algorithms for hyper-parameter optimization. *Advances in neural information processing systems*, 24, 2011.
- Bradford, E., Schweidtmann, A. M., and Lapkin, A. Efficient multiobjective optimization employing gaussian processes, spectral sampling and a genetic algorithm. *Journal of global optimization*, 71(2):407–438, 2018.
- Cheng, F. and Li, X. Generalized center method for multiobjective engineering optimization. *Engineering Optimization*, 31(5):641–661, 1999.
- Cornish, R., Caterini, A., Deligiannidis, G., and Doucet, A. Relaxing bijectivity constraints with continuously indexed normalising flows. In *International conference on machine learning*, pp. 2133–2143. PMLR, 2020.
- Couckuyt, I., Deschrijver, D., and Dhaene, T. Fast calculation of multiobjective probability of improvement and expected improvement criteria for pareto optimization. *Journal of Global Optimization*, 60:575–594, 2014.
- Daulton, S., Balandat, M., and Bakshy, E. Differentiable expected hypervolume improvement for parallel multi-objective bayesian optimization. *Advances in Neural Information Processing Systems*, 33:9851–9864, 2020.
- Daulton, S., Balandat, M., and Bakshy, E. Parallel bayesian optimization of multiple noisy objectives with expected hypervolume improvement. *Advances in Neural Information Processing Systems*, 34:2187–2200, 2021.

- Deb, K. and Srinivasan, A. Innovization: Innovating design principles through optimization. In *Proceedings of the 8th annual conference on Genetic and evolutionary computation*, pp. 1629–1636, 2006.
- Deb, K., Pratap, A., Agarwal, S., and Meyarivan, T. A fast and elitist multiobjective genetic algorithm: Nsga-ii. *IEEE transactions on evolutionary computation*, 6(2): 182–197, 2002.
- Deb, K., Thiele, L., Laumanns, M., and Zitzler, E. *Scalable test problems for evolutionary multiobjective optimization*. Springer, 2005.
- Dhariwal, P. and Nichol, A. Diffusion models beat gans on image synthesis. *Advances in Neural Information Processing Systems*, 34:8780–8794, 2021a.
- Dhariwal, P. and Nichol, A. Diffusion models beat gans on image synthesis. *Advances in neural information processing systems*, 34:8780–8794, 2021b.
- Ding, D., Li, D., Li, Z., and Yang, L. Compact circularly-polarized microstrip antenna for hand-held rfid reader. In *2019 8th Asia-Pacific Conference on Antennas and Propagation (APCAP)*, pp. 181–182. IEEE, 2019.
- Dung, D. A. and Binh, H. T. T. Gdegan: Graphical discriminative embedding gan for tabular data. In *2022 IEEE 9th International Conference on Data Science and Advanced Analytics (DSAA)*, pp. 1–11. IEEE, 2022.
- Fang, W., Du, W., He, R., Tang, Y., Jin, Y., and Yen, G. G. Diffusion model-based multiobjective optimization for gasoline blending scheduling. *arXiv preprint arXiv:2402.14600*, 2024.
- Gong, M., Xu, Y., Li, C., Zhang, K., and Batmanghelich, K. Twin auxiliary classifiers gan. *Advances in neural information processing systems*, 32, 2019.
- Ho, J. and Salimans, T. Classifier-free diffusion guidance. *arXiv preprint arXiv:2207.12598*, 2022.
- Ho, J., Jain, A., and Abbeel, P. Denoising diffusion probabilistic models. *Advances in neural information processing systems*, 33:6840–6851, 2020.
- Ho, J., Chan, W., Saharia, C., Whang, J., Gao, R., Gritsenko, A., Kingma, D. P., Poole, B., Norouzi, M., Fleet, D. J., et al. Imagen video: High definition video generation with diffusion models. *arXiv preprint arXiv:2210.02303*, 2022.
- Hoffman, M. W. and Ghahramani, Z. Output-space predictive entropy search for flexible global optimization. In *NIPS workshop on Bayesian Optimization*, pp. 1–5, 2015.
- Jin, C., Netrapalli, P., Ge, R., Kakade, S. M., and Jordan, M. I. On nonconvex optimization for machine learning: Gradients, stochasticity, and saddle points. *Journal of the ACM (JACM)*, 68(2):1–29, 2021.
- Jones, D. R., Schonlau, M., and Welch, W. J. Efficient global optimization of expensive black-box functions. *Journal of Global optimization*, 13(4):455, 1998.
- Kang, M., Shim, W., Cho, M., and Park, J. Rebooting acgan: Auxiliary classifier gans with stable training. *Advances in neural information processing systems*, 34:23505–23518, 2021.
- Kannan, B. and Kramer, S. N. An augmented lagrange multiplier based method for mixed integer discrete continuous optimization and its applications to mechanical design. 1994.
- Knowles, J. Parego: A hybrid algorithm with on-line landscape approximation for expensive multiobjective optimization problems. *IEEE Transactions on Evolutionary Computation*, 10(1):50–66, 2006.
- Konakovic Lukovic, M., Tian, Y., and Matusik, W. Diversity-guided multi-objective bayesian optimization with batch evaluations. *Advances in Neural Information Processing Systems*, 33:17708–17720, 2020.
- Krishnamoorthy, S., Mashkaria, S. M., and Grover, A. Diffusion models for black-box optimization. In *International Conference on Machine Learning*, pp. 17842–17857. PMLR, 2023.
- Laumanns, M. and Ocenasek, J. Bayesian optimization algorithms for multi-objective optimization. In *Parallel Problem Solving from Nature—PPSN VII: 7th International Conference Granada, Spain, September 7–11, 2002 Proceedings 7*, pp. 298–307. Springer, 2002.
- Leng, Y., Chen, Z., Guo, J., Liu, H., Chen, J., Tan, X., Mandic, D., He, L., Li, X., Qin, T., et al. Binauralgrad: A two-stage conditional diffusion probabilistic model for binaural audio synthesis. *Advances in Neural Information Processing Systems*, 35:23689–23700, 2022.
- Letham, B., Karrer, B., Ottoni, G., and Bakshy, E. Constrained bayesian optimization with noisy experiments. 2019.
- Li, M., Yang, S., and Liu, X. Shift-based density estimation for pareto-based algorithms in many-objective optimization. *IEEE Transactions on Evolutionary Computation*, 18(3):348–365, 2013.
- Lin, X., Yang, Z., Zhang, X., and Zhang, Q. Pareto set learning for expensive multi-objective optimization. In *36th Conference on Neural Information Processing Systems (NeurIPS 2022)*, 2022.

- Liu, J., Li, C., Ren, Y., Chen, F., and Zhao, Z. DiffSinger: Singing voice synthesis via shallow diffusion mechanism. In *Proceedings of the AAAI conference on artificial intelligence*, volume 36, pp. 11020–11028, 2022.
- Liu, X., Park, D. H., Azadi, S., Zhang, G., Chopikyan, A., Hu, Y., Shi, H., Rohrbach, A., and Darrell, T. More control for free! image synthesis with semantic diffusion guidance. In *Proceedings of the IEEE/CVF Winter Conference on Applications of Computer Vision*, pp. 289–299, 2023.
- Lu, Z., Whalen, I., Boddeti, V., Dhebar, Y., Deb, K., Goodman, E., and Banzhaf, W. Nsga-net: neural architecture search using multi-objective genetic algorithm. In *Proceedings of the genetic and evolutionary computation conference*, pp. 419–427, 2019.
- Lugmayr, A., Danelljan, M., Romero, A., Yu, F., Timofte, R., and Van Gool, L. Repaint: Inpainting using denoising diffusion probabilistic models. In *Proceedings of the IEEE/CVF Conference on Computer Vision and Pattern Recognition*, pp. 11461–11471, 2022.
- McKay, M. D., Beckman, R. J., and Conover, W. J. A comparison of three methods for selecting values of input variables in the analysis of output from a computer code. *Technometrics*, 42(1):55–61, 2000.
- Močkus, J. On bayesian methods for seeking the extremum. In *Optimization Techniques IFIP Technical Conference: Novosibirsk, July 1–7, 1974*, pp. 400–404. Springer, 1975.
- Odena, A., Olah, C., and Shlens, J. Conditional image synthesis with auxiliary classifier gans. In *International conference on machine learning*, pp. 2642–2651. PMLR, 2017.
- Preechakul, K., Chatthee, N., Wizadwongsa, S., and Suwanajakorn, S. Diffusion autoencoders: Toward a meaningful and decodable representation. In *Proceedings of the IEEE/CVF Conference on Computer Vision and Pattern Recognition*, pp. 10619–10629, 2022.
- Ray, T. and Liew, K. A swarm metaphor for multiobjective design optimization. *Engineering optimization*, 34(2): 141–153, 2002.
- Shahriari, B., Swersky, K., Wang, Z., Adams, R. P., and De Freitas, N. Taking the human out of the loop: A review of bayesian optimization. *Proceedings of the IEEE*, 104(1):148–175, 2015.
- Shannon, C. E. A mathematical theory of communication. *The Bell system technical journal*, 27(3):379–423, 1948.
- Snoek, J., Larochelle, H., and Adams, R. P. Practical bayesian optimization of machine learning algorithms. *Advances in neural information processing systems*, 25, 2012.
- Sohl-Dickstein, J., Weiss, E., Maheswaranathan, N., and Ganguli, S. Deep unsupervised learning using nonequilibrium thermodynamics. In *International conference on machine learning*, pp. 2256–2265. PMLR, 2015.
- Song, L., Xue, K., Huang, X., and Qian, C. Monte carlo tree search based variable selection for high dimensional bayesian optimization. *Advances in Neural Information Processing Systems*, 35:28488–28501, 2022.
- Song, Y., Sohl-Dickstein, J., Kingma, D. P., Kumar, A., Ermon, S., and Poole, B. Score-based generative modeling through stochastic differential equations. *arXiv preprint arXiv:2011.13456*, 2020.
- Tanabe, R. and Ishibuchi, H. An easy-to-use real-world multi-objective optimization problem suite. *Applied Soft Computing*, 89:106078, 2020.
- Vaidyanathan, R., Tucker, K., Papila, N., and Shyy, W. Cfd-based design optimization for single element rocket injector. In *41st Aerospace sciences meeting and exhibit*, pp. 296, 2003.
- Wu, H., Köhler, J., and Noé, F. Stochastic normalizing flows. *Advances in Neural Information Processing Systems*, 33: 5933–5944, 2020.
- Yan, X. and Jin, Y. Emodm: A diffusion model for evolutionary multi-objective optimization. *arXiv preprint arXiv:2401.15931*, 2024.
- Yang, L., Zhang, Z., Song, Y., Hong, S., Xu, R., Zhao, Y., Zhang, W., Cui, B., and Yang, M.-H. Diffusion models: A comprehensive survey of methods and applications. *ACM Computing Surveys*, 56(4):1–39, 2023.
- Yu, P.-L. Cone convexity, cone extreme points, and non-dominated solutions in decision problems with multiobjectives. *Journal of optimization Theory and Applications*, 14:319–377, 1974.
- Yu, S., Tack, J., Mo, S., Kim, H., Kim, J., Ha, J.-W., and Shin, J. Generating videos with dynamics-aware implicit generative adversarial networks. *arXiv preprint arXiv:2202.10571*, 2022.
- Yu, Z., Ramakrishnan, V., and Meinzer, C. Simulation optimization for bayesian multi-arm multi-stage clinical trial with binary endpoints. *Journal of Biopharmaceutical Statistics*, 29(2):306–317, 2019.
- Zhang, Q., Liu, W., Tsang, E., and Virginas, B. Expensive multiobjective optimization by moea/d with gaussian process model. *IEEE Transactions on Evolutionary Computation*, 14(3):456–474, 2009.

- Zhang, Y., Sohn, K., Villegas, R., Pan, G., and Lee, H. Improving object detection with deep convolutional networks via bayesian optimization and structured prediction. In *Proceedings of the IEEE Conference on Computer Vision and Pattern Recognition (CVPR)*, June 2015.
- Zhao, Y., Li, C., Yu, P., Gao, J., and Chen, C. Feature quantization improves gan training. *arXiv preprint arXiv:2004.02088*, 2020.
- Zitzler, E. and Thiele, L. Multiobjective evolutionary algorithms: a comparative case study and the strength pareto approach. *IEEE transactions on Evolutionary Computation*, 3(4):257–271, 1999.
- Zitzler, E., Deb, K., and Thiele, L. Comparison of multiobjective evolutionary algorithms: Empirical results. *Evolutionary computation*, 8(2):173–195, 2000.
- Zoph, B., Vasudevan, V., Shlens, J., and Le, Q. V. Learning transferable architectures for scalable image recognition. In *Proceedings of the IEEE conference on computer vision and pattern recognition*, pp. 8697–8710, 2018.

A. Experimental Details

A.1. Parameter Settings

First, we supplement more details about training DM. DM is designed with a straightforward architecture, incorporating two linear layers, each containing 128 hidden units, and utilizes the ReLU activation function. Additionally, we train DM for 4000 epochs, with a batch size of 1024. The Adam optimizer is selected for the model, set with a learning rate of 0.0001.

Moreover, the hyperparameter for the DM’s step t is configured at 25, and the noise level is defined within the range from $1e-5$ to $0.5e-1$.

The maximum number of function evaluations is 200, where 100 FEs are used to initialize the population and 100 FEs are used to evaluate new offspring after batch selection. Besides, batch size of all the algorithms is 5, thus number of iterations is $100 / 5 = 20$.

In CDM-PSL, the initial populations are all obtained from the Latin Hypercube Sampling (LHS) (McKay et al., 2000). To ensure fairness and allow the comparison algorithms to perform as them originally did, the relevant settings of the comparison algorithms are kept unchanged from the original paper.

A.2. Synthetic Benchmark Problems

In this subsection, we detail each synthetic benchmark problem, outlining the dimensions of the decision space $\mathcal{X} \in \mathbb{R}^d$ and the objective space $\mathbf{f}(\mathcal{X}) \in \mathbb{R}^M$, where $\mathbf{f}(\cdot)$ represents the black-box function. Additionally, we discuss the reference points \mathbf{r} utilized for computing the hypervolume indicator. Our experiments encompass 9 synthetic benchmark problems, with the objectives numbering 2 and 3, and the decision variables is 10, 20 and 50. Further details are available in Table 1, and the characteristics of each problem are listed in Table 2. For the reference point $\mathbf{r} \in \mathbb{R}^M$, we adopt a vector comprising the maximum objective values from the initial solution set $\mathbf{x}_1, \dots, \mathbf{x}_N$ (Eq. 12).

$$\mathbf{r} = (\max_{1 \leq i \leq N} \mathbf{f}_1(\mathbf{x}_i), \dots, \max_{1 \leq i \leq N} \mathbf{f}_M(\mathbf{x}_i)) \quad (12)$$

A.3. Real-world Application Problems

Our experiments include 7 real-world application problems (Tanabe & Ishibuchi, 2020), alongside several synthetic benchmark problems. These problems were originally proposed across various fields for distinct applications. Below are introductions to each of these real-world problems:

Four Bar Truss Design (RE1). This task aims to optimize the design of a four-bar truss, focusing on minimizing structural volume (f_1) and joint displacement (f_2). It considers the lengths of the four bars (x_1, x_2, x_3 , and x_4) as variables. For more information, please see (Cheng & Li, 1999).

Pressure Vessel Design (RE2). The goal here is to design a cylindrical pressure vessel to minimize total costs (f_1), including materials, forming, and welding, and to avoid violations of three design constraints (f_2). The decision variables are the shell thicknesses (x_1), the pressure vessel head (x_2), the inner radius (x_3), and the length of the cylindrical section (x_4). Additional details are in (Kannan & Kramer, 1994).

Disk Brake Design (RE3). This problem focuses on designing a disc brake to minimize mass (f_1), stopping time (f_2), and violations of four design constraints (f_3), with four decision variables: inner radius (x_1), outer radius (x_2), engaging force (x_3), and the number of friction surfaces (x_4). Further details are available in (Ray & Liew, 2002).

Gear Train Design (RE4). The objective is to design a gear train to minimize the deviation from the required gear ratio (f_1), the maximum size of the gears (f_2), and violations of design constraints (f_3), considering the number of teeth in each of the four gears (x_1, x_2, x_3 , and x_4). More information can be found in (Deb & Srinivasan, 2006).

Rocket Injector Design (RE5). The design goal for the rocket injector is to minimize the maximum temperature on the injector face (f_1), the distance from the inlet (f_2), and the temperature at the post tip (f_3), with decision variables including

Table 1. Description of synthetic benchmarks we used in this work.

Problem	M	d	reference point (r)
ZDT1	10	2	(0.9901, 5.8380)
	20	2	(0.9994, 6.0576)
	50	2	(0.9926, 5.8722)
ZDT2	10	2	(0.9901, 7.4625)
	20	2	(0.9994, 6.8960)
	50	2	(0.9926, 6.2181)
ZDT3	10	2	(0.9901, 5.8101)
	20	2	(0.9994, 6.0571)
	50	2	(0.9926, 5.8648)
DTLZ2	10	3	(1.8753, 1.9635, 2.0503)
	20	3	(2.8390, 2.9011, 2.8575)
	50	3	(5.4059, 5.6415, 6.5147)
DTLZ3	10	3	(1002.2772, 1173.7753, 1075.0803)
	20	3	(2421.6427, 1905.2767, 2532.9691)
	50	3	(5298.0203, 5548.5643, 6250.5483)
DTLZ4	10	3	(2.1527, 1.2691, 0.9761)
	20	3	(3.2675, 2.6443, 2.4263)
	50	3	(6.9024, 4.2313, 3.61552)
DTLZ5	10	3	(1.7079, 1.7896, 2.0503)
	20	3	(2.6672, 2.8009, 2.8575)
	50	3	(5.2481, 5.5483, 6.5147)
DTLZ6	10	3	(8.1417, 8.0853, 8.5711)
	20	3	(16.8258, 16.9194, 17.7646)
	50	3	(42.4261, 44.4857, 45.2363)
DTLZ7	10	3	(0.9902, 0.9932, 24.5440)
	20	3	(0.9984, 0.9961, 22.8114)
	50	3	(0.9925, 0.9954, 21.7584)

hydrogen flow angle (x_1), hydrogen area (x_2), oxygen area (x_3), and oxidizer post tip thickness (x_4). Detailed information is in (Vaidyanathan et al., 2003).

Reinforced Concrete Beam Design (RE6). This design problem for a reinforced concrete beam aims to minimize the total cost of concrete and reinforcing steel (f_1) and the sum of two constraint violations (f_2), with variables for the reinforcement area (x_1), beam width (x_2), and beam depth (x_3). Details are available in (Amir & Hasegawa, 1989).

Welded Beam Design (RE7). The challenge is to design a welded beam to minimize the cost (f_1), end deflection (f_2), and violations of four constraints (f_3), with variables adjusting the beam's size (x_1 , x_2 , x_3 , and x_4). More information can be found in (Ray & Liew, 2002).

To maintain consistency in evaluation, the same reference point was applied when evaluating all the algorithms. More details are shown in the supplementary material. Details on the real-world application problems, including information and reference points, are presented in Table 3.

Table 2. Characteristics of the synthetic benchmark problems.

Benchmark problem	Features of Pareto front	Features of landscape	Separability of objective functions
DTLZ1	Linear	Multimodal	Fully Separable
DTLZ2	Concave	Unimodal	Fully Separable
DTLZ3	Concave	Multimodal	Fully Separable
DTLZ4	Concave	Unimodal, biased	Fully Separable
DTLZ5	Concave, degenerate	Unimodal	Fully Separable
DTLZ6	Concave, degenerate	Unimodal, biased	Fully Separable
DTLZ7	Disconnected	Multimodal	Fully Separable

Table 3. Description of real-world application problems we used in this work.

Problem	d	M	reference point (r)
RE1	4	2	(2763.2229, 0.0369)
RE2	4	2	(528107.1899, 1279320.8107)
RE3	4	3	(7.6853, 7.2861, 21.5010)
RE4	4	3	(6.7921, 60.0, 0.48)
RE5	4	3	(0.8745, 1.05092, 1.0533)
RE6	3	2	(749.9241, 2229.3748)
RE7	4	3	(210.3363, 1069.9160, 39196770.1704)

A.4. Hardware Settings

The experiments in this paper are conducted on a server with Ubuntu 22.04 LTS operating system, a 1.5GHz AMD EPYC 7742 CPU (64 CPU Cores), 320 GB RAM, and two NVIDIA RTX 4090 GPU.

B. Related Works

B.1. Comparing DM-Based Methods with Normalizing Flows

Normalizing flows (NF) transforms data into a prior distribution through bijective functions, which limits the ability of modeling complex data distribution in both practical and theoretical contexts (Cornish et al., 2020; Wu et al., 2020). However, DM is more efficient in the task of **capturing complex data distributions**, and the CDM-PSL proposed in this paper also demonstrates this experimentally. Moreover, the random noise introduced by DM can also naturally **generates a greater diversity of candidate solutions**.

Specifically, DM enhances its expressive power by introducing random noise in the forward and backward processes, compared with NF. Considering the case of generating candidate solutions, this property of DM enables the exploration of more solutions in the space, thus enriching the diversity of solutions.

From the perspective of the motivation behind our proposed method, the performance of PSL methods might deteriorate significantly due to the complexity of distributions of Pareto optimal solutions and the limitation of function evaluations in the face of EMOBOPs. **DM can model complex distributions of solutions step by step, and generate more diverse solutions by introducing random noise**. This gives DM an advantage over NF for application on the PSL of EMOBOPs.

B.2. Comparing CDM-PSL with DDOM

In this section, we explain the novelty and advantages of CDM over DDOM. Krishnamoorthy proposed an offline black-box optimization algorithm named DDOM (Krishnamoorthy et al., 2023), based on the diffusion model. DDOM trains a generative model on offline dataset and proof its effectiveness on single-objective optimization problems. The novelty and advantages of CDM-PSL over DDOM are as follows:

Model composition: The main difference between CDM-PSL and DDOM is that CDM consists of two generative models, CG and UG. CG can minimize all the objective values as much as possible in a limited number of function evaluations, and UG can generate solutions with greater diversity.

Training data: CDM-PSL trains DM on online dataset, while DDOM is trained on offline dataset, which means that CDMs are able to receive and learn new data instantly, which allows them to quickly adapt to changes in data distribution.

Inference process: CDM-PSL introduces gradient information, weighted by information entropy, into the process of generating solutions, significantly enhancing convergence performance under limited FEs.

Research problems: CDM-PSL is targeted at solving multi-objective optimization problems, while DDOM mainly solves single-objective optimization problems.

The combination of our proposed methods makes CDM-PSL have competitive performance in solving EMOPs.

C. Additional Experiments

C.1. The Advantages of Using Diffusion Model

Effectively modeling the complicated distribution of the PS is quite challenging for EMOPs with limited function evaluations. Existing Pareto set learning algorithms may exhibit considerable instability in expensive scenarios (Lin et al., 2022). DM is meticulously engineered to represent complex datasets through a highly flexible family of probability distributions. It has demonstrated promising outcomes in several domains, notably in image restoration and data synthesis (Sohl-Dickstein et al., 2015). Thus, DM offers a promising way for Pareto set learning in expensive multi-objective Bayesian optimization. Specifically, the proposed CDM-PSL is a composite of CG with conditional DM and UG with unconditional DM. It takes advantage of **CG’s convergence capabilities with UG’s diversity potential**. Figure 6 illustrates the offspring produced by the SBX versus those generated by CG and UG on DTLZ7 and ZDT1 at FE = 25. The closer to (0, 0, 0), the better. As can be seen from the figure, both CG and UG can generate solutions with lower objective values.

- **CG with conditional DM** can generate offspring solutions closer to the PF than SBX and UG by introducing performance gradient information in the denoising process, i.e., it **has stronger convergence performance**.
- **UG with unconditional DM** does not have as strong convergence performance as CG, but since it does not rely on the gradient of the aggregated objective values to guide the denoising process, the solutions generated by UG will **have stronger diversity**.

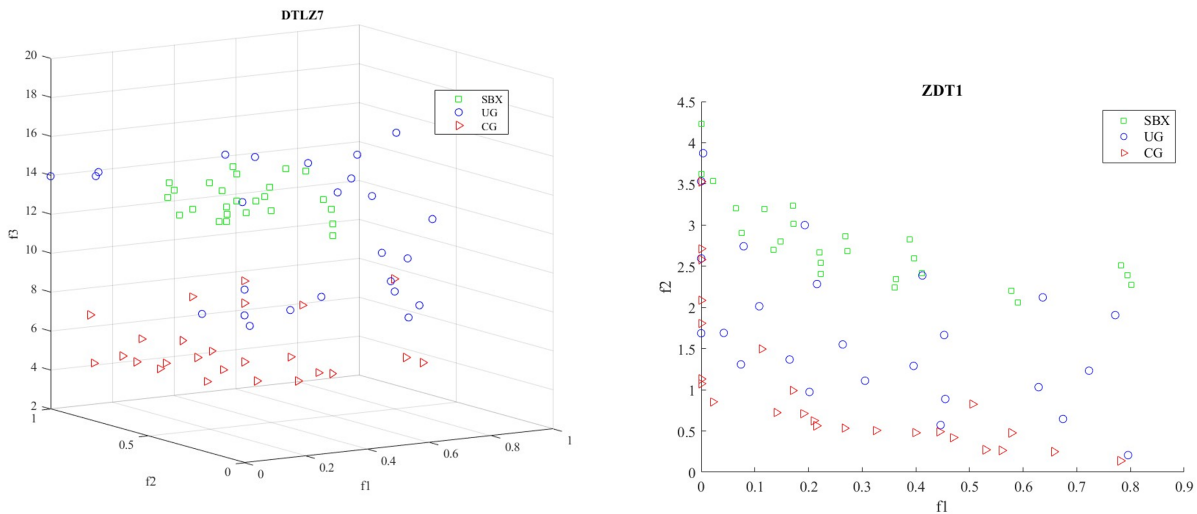


Figure 6. The objective values of newly generated solutions obtained by GA’s SBX method, UG and CG. ($d = 20, FE = 25$)

C.2. The Advantages of Entropy Weighting Method

The entropy weighting method, serving as an adaptive weight allocation approach, assigns weights based on the information entropy of objectives. This method reduces subjectivity in weighting gradients for different objective values, and **ensures that the algorithm places more emphasis on objectives with rich information content**, thereby achieving **better performance in multi-objective optimization problems**.

To show the advantages of entropy weighting method, we visualize the offspring to compare the convergence performance of SBX and CG under three different weighting methods: entropy weighting, mean weighting, and random weighting. Figure 7 illustrates the objective values of all newly generated solutions at $FE = 25$. As can be seen from the figure, CG with weights can generate solutions with lower objective values across multiple objectives. Moreover, **CG with entropy weighted gradient has better convergence performance** compared to others. This is because CG (entropy weight) pay close attention to objectives that are relatively more important (with higher information entropy) during the generation of offspring. The offspring produced by it exhibit **stronger convergence** compared to those generated with CG (mean weight) and CG (random weight).

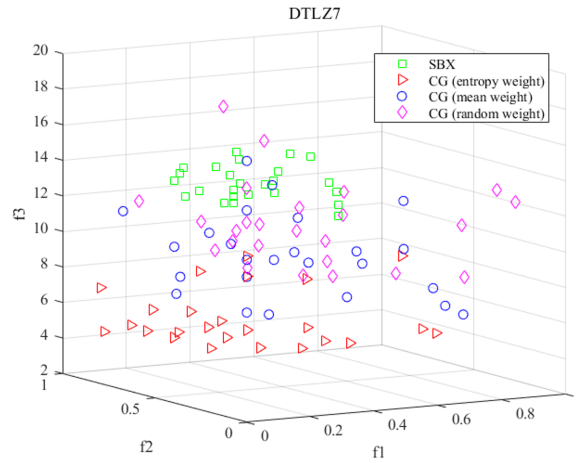


Figure 7. The objective values of newly generated solutions obtained by GA’s SBX method, CG(entropy weight), CG(mean weight) and CG(random weight). ($d = 20$, $FE = 25$)

C.3. The Advantages of CDM Over a Gradient-Based Method With Multiple Restarts

In this section, we demonstrate through experiments the advantages of our proposed CDM-PSL compared to the gradient-based method (GM) with multiple restarts. The main advantage of CDM over gradient-based methods is that CDM is based on **population-wide information** to generate new offsprings, while some other general optimization methods are based on **individual solutions** to generate new offsprings and they **ignore the connections between solutions**, which makes CDM more advantageous in maintaining population diversity (Lin et al., 2022).

Moreover, gradient-based methods are more likely to **get stuck in local optima or saddle points** and fail to explore the global optimum, and **they are sensitive to the choice of the initial point and the step size** (Jin et al., 2021). While the problem of them falling into a local optimum can be mitigated to some extent by restart, this can lead to significant time overhead when dealing with high dimensional problem. However, **DM can model complex distributions of solutions**, and generate more diverse solutions by introducing random noise.

To compare the performance of CDM and GM through experiments, we implemented a GM with multiple restarts, with the following specific settings:

- The objective value gradient of the current solution is obtained in the same manner as in CG.
- The weighting of the gradient adopts the entropy weighting method, which is the most effective in CG.

- SDE is used to select good solutions for the next generation of offspring through gradient methods.
- Data augmentation is performed on the selected solutions (starting points for the gradient method), including adding Gaussian noise/random perturbations, etc.

The experimental results are shown in Figure 8 ($d = 20, FE = 25$), which validate the advantages of CDM over GM with multiple restarts by visualizing the offspring. GM generates solutions that are more likely to fall into local optimality, while CDM can maintain better diversity.

Figure 9 demonstrates that **CDM, compared with GM, can generate solutions with better convergence and diversity** by comparing the HV values of both.

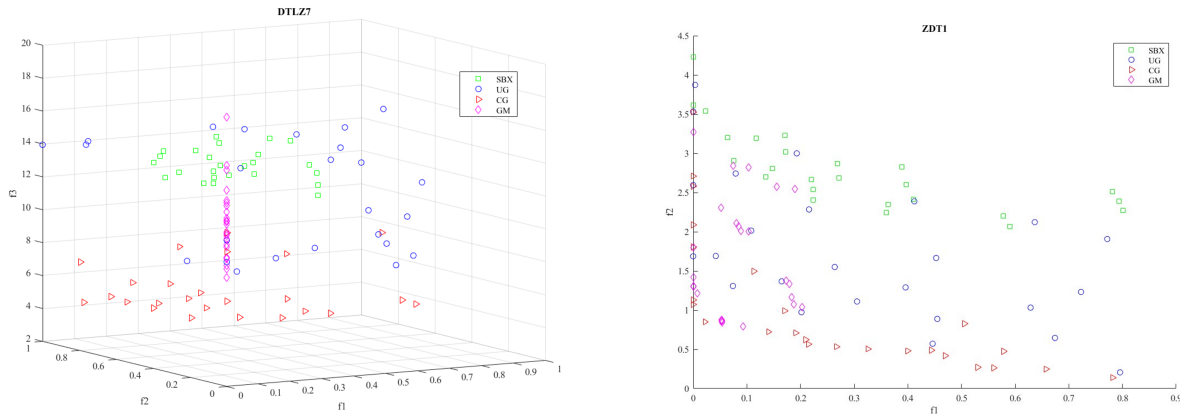


Figure 8. The objective values of newly generated solutions obtained by GA’s SBX method, UG, CG and GM. ($d = 20, FE = 25$)

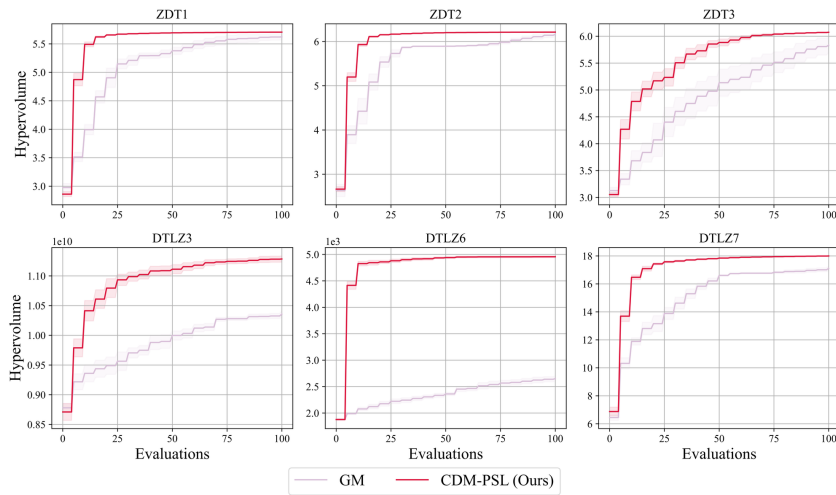


Figure 9. The HV results of CDM-PSL and GM ($d = 20$).

C.4. Results on Synthetic Benchmark Problems with Various Decision Space Scales

In this section, we broaden our experimental scope to encompass problems within 10-dimensional decision spaces, maintaining the same experimental parameters as before, including a batch size of 5, 20 iterations, and an initial sample size of 100. The outcomes, illustrated in Figure 10 and 11, also demonstrate that, overall, CDM-PSL is superior to the methods compared.

Specifically, when the dimensionality of decision variables is set to 10, CDM-PSL exhibits highly competitive performance in almost all problems compared to the benchmark methods. Furthermore, when the dimensionality of decision variables reaches 50, our proposed method achieves notably superior performance on DTLZ2, DTLZ4, DTLZ5, and DTLZ6. However, the performance of CDM-PSL shows some degradation on ZDT3, DTLZ3, and DTLZ7. As indicated by the characteristics of benchmark problems in Table 2, these problems all possess a multimodal landscape feature. This phenomenon occurs because our proposed Pareto set learning approach generates new offspring based on the distribution of the current population. In these three types of problems, the Pareto optimal set is distributed across multiple regions, and with the increase in decision space dimensionality, the Pareto optimal sets of these multimodal landscape problems become more complex. As a result, our method might struggle with adequate exploration and exploitation on these types of problems at higher dimensions. In contrast, CDM-PSL excels in capturing unimodal Pareto sets (such as DTLZ2, DTLZ4, DTLZ5, and DTLZ6), particularly in high-dimensional decision spaces, showing a clear advantage over the methods compared.

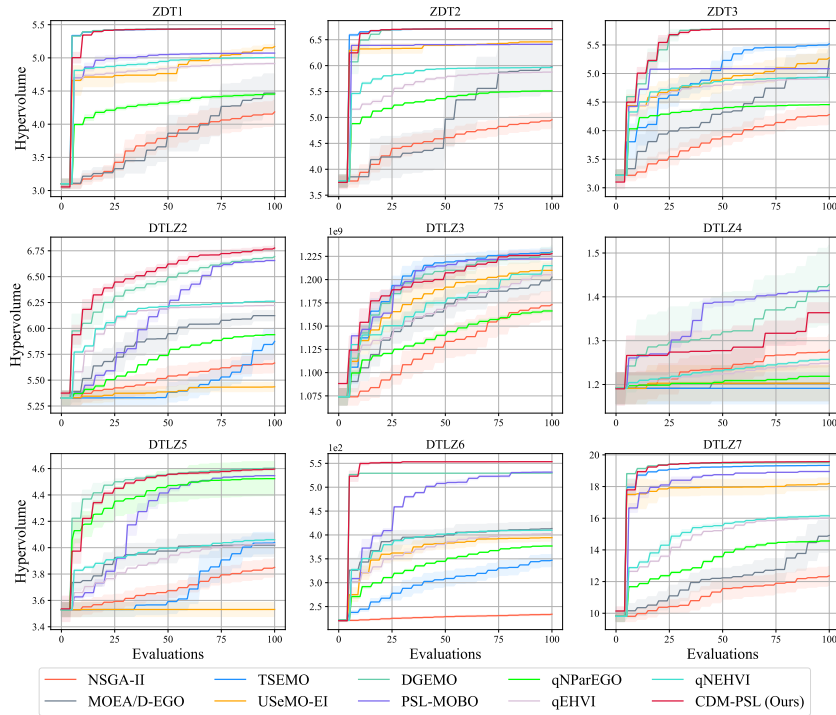


Figure 10. The HV results of 10 algorithms, evaluated on synthetic test functions and real-world problems ($d = 10$).

C.5. Results on Synthetic Benchmark Problems with Various Initial population size

In this section, we experiment with the performance of CDM-PSL under varying initial population sizes. We selected qEHVI (Daulton et al., 2020), qNEHVI (Daulton et al., 2021), qLogEHVI (Ament et al., 2024), and qLogNEHVI (Ament et al., 2024) as comparison algorithms. The initial population size for these algorithms were set according to their default settings, specifically $2(d + 1)$, where d represents the dimension of the solution. Figure 12 presents the results of these five algorithms on different problems. From the figure, it is evident that even with a smaller initial population size, CDM-PSL maintains good convergence performance in the early stages of the algorithm. Furthermore, compared to the other algorithms, CDM-PSL achieves higher HV values in the final evaluation.

C.6. Comparison of Log HV Differences

In this section, we include the plot of log HV difference for all the test problems ($d = 20$). Figure 13 shows the plots of log HV difference for CDM-PSL (our method) alongside PSL-MOBO and DGEMO, which are two of the most competitive algorithms examined in our experiments. This comparison effectively highlights what fraction of the problem was actually solved and showcase the superior performance of CDM-PSL.

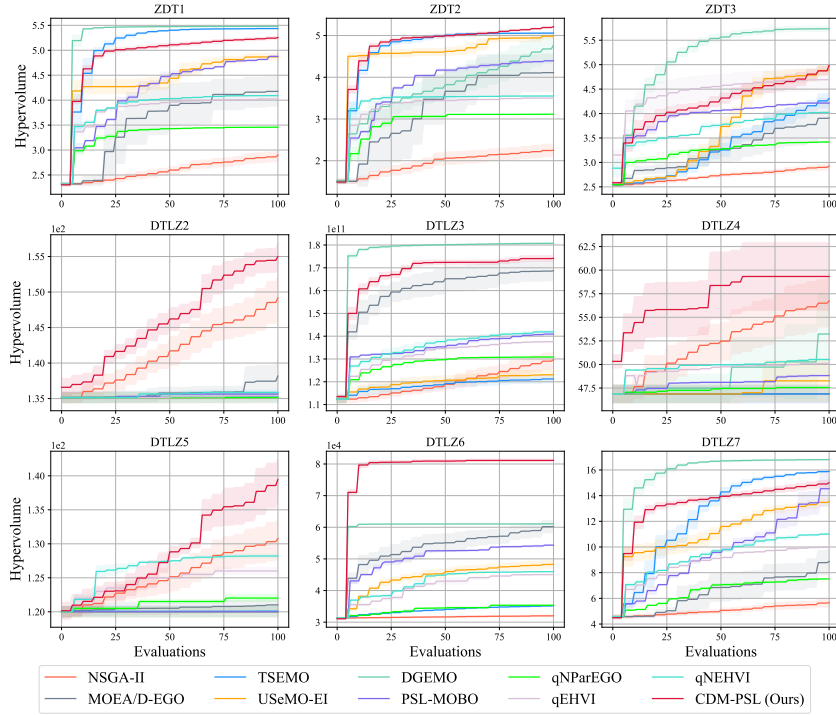


Figure 11. The HV results of 10 algorithms, evaluated on synthetic test functions and real-world problems ($d = 50$).

C.7. Ablation Study with Limited FEs

To analyze the convergence performance of our proposed method, we compare CDM-PSL with three variants: CDM-PSL without entropy weight (CDM-PSL w/o Weight), CDM-PSL without conditional generation (CDM-PSL w/o Condition), CDM-PSL without diffusion model (CDM-PSL w/o DM). As can be seen from the Table 4, the convergence performance of CDM-PSL is impaired when any of the components is ablated. Notably, incorporating the diffusion model to generate offspring significantly improves the model’s performance with a minimal number of function evaluations (specifically, 25), enabling it to achieve higher HV values within a limited set of evaluations.

Table 4. Comparison of HV Values for CDM-PSL and its variants at 25 FEs.

Method	ZDT1		ZDT2		ZDT3		DTLZ3		DTLZ6		DTLZ7	
	HV \uparrow	Gap \downarrow	HV \uparrow	Gap \downarrow	HV \uparrow	Gap \downarrow	HV \uparrow	Gap \downarrow	HV \uparrow	Gap \downarrow	HV \uparrow	Gap \downarrow
CDM-PSL w/o Weight	4.9542e+00	12.42%	5.4062e+00	12.14%	4.2659e+00	17.49%	1.0391e+10	3.74%	4.3509e+03	10.46%	1.4604e+01	16.22%
CDM-PSL w/o Condition	4.9587e+00	12.34%	5.1008e+00	17.10%	4.1583e+00	19.57%	1.0420e+10	3.47%	4.2265e+03	13.02%	1.4622e+01	16.12%
CDM-PSL w/o DM	3.6577e+00	34.35%	3.7327e+00	39.34%	3.7185e+00	28.08%	9.6465e+09	10.64%	2.2088e+03	54.54%	9.4968e+00	45.52%
CDM-PSL	5.6570e+00	0.00%	6.1533e+00	0.00%	5.1703e+00	0.00%	1.0795e+10	0.00%	4.8592e+03	0.00%	1.7432e+01	0.00%

C.8. Pareto Fronts Obtained by CDM-PSL on Real-World Problems

In this section, we add more figures of the final solutions obtained by CDM-PSL in Real-World Problems. As can be seen from the figures 14, the proposed CDM-PSL can effectively modeling the distribution of the PS, despite that the Pareto fronts of the real-world test problems RE1-RE7 are complicated.

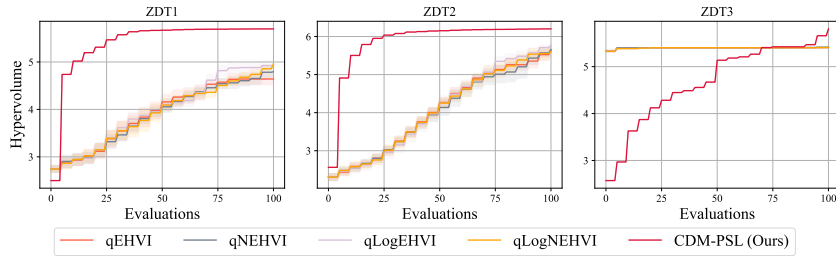


Figure 12. The HV results of 5 algorithms, with the initial population size of $2(d + 1)$, where $d = 20$.

C.9. Parameter Analysis

C.9.1. PERFORMANCE WITH DIFFERENT LEARNING RATES

In this section we compare the performance of CDM-PSL under different learning rate settings to validate the sensitivity of our proposed method to this parameter. Figure 15 illustrates the impact of varying learning rates on the performance of CDM-PSL, notably with $lr = 0.001$ being the default setting of our proposed method. The results depicted in Figure 15 indicate that there are no significant differences in the performance of CDM-PSL across different learning rates.

C.9.2. STUDY OF CG AND UG RATIOS IN CDM-PSL

In this section we explore the impact of varying ratios between conditional generation and unconditional generation in CDM-PSL. Figure 16 displays the HV values for CDM-PSL with different CG and UG ratios across multiple problems. Here, "C1-U10" signifies a CG to UG ratio of 1 to 10, which is the default setting for CDM-PSL; "C3-U8" indicates a ratio of 3 to 8; and so forth. From the figure, it is observable that incrementing the proportion of CG from the default configuration marginally improves the algorithm's early convergence performance, as evidenced by a slightly elevated HV value up to the 25th function evaluation. However, with a sufficient number of function evaluations, the DM has been able to learn the distribution of the good solutions more accurately. Consequently, the optimal final HV value is achievable with a minimal CG ratio and a predominately higher experimental group UG ratio. Therefore, we opt for a CG to UG ratio of 1 to 10, which significantly reduces the algorithm's time overhead without compromising its final performance.

C.10. Time overhead of CDM-PSL

We choose ZDT1 and DTLZ2 to discuss the time overhead of CDM-PSL, the number of decision variables is 10 and 20 respectively, the maximum number of function evaluations is set to 120, and the parameters for training CDM are consistent with the default settings mentioned in the manuscript.

Table 5 lists the time overhead of each part of the CDM-PSL, including training, CG, UG and others. We choose ZDT1 and DTLZ2 to discuss the time overhead of the algorithms, the number of decision variables is 10 and 20 respectively, the maximum number of function evaluations is set to 120, and the parameters for training CDM are consistent with the default settings mentioned in the manuscript.

As we can see from the table, the time overhead of training DM is a relatively modest fraction of the total time overhead of CDM-PSL. CG takes longer to generate new candidate solutions compared to UG. This significant difference is attributed to CG's reliance on a surrogate model to calculate the objective values during the denoising process, which is essential for obtaining the gradient information needed to guide the denoising. However, the additional time overhead imposed by CDM is acceptable compared to the rest of the algorithm.

In the far right column of the table, we present the time overhead associated with one of the latest SOTA algorithms, PSL-MOBO. A comparison between the total time overhead of our method and that of PSL-MOBO indicates that the additional time overhead incurred by CDM is within acceptable limits.

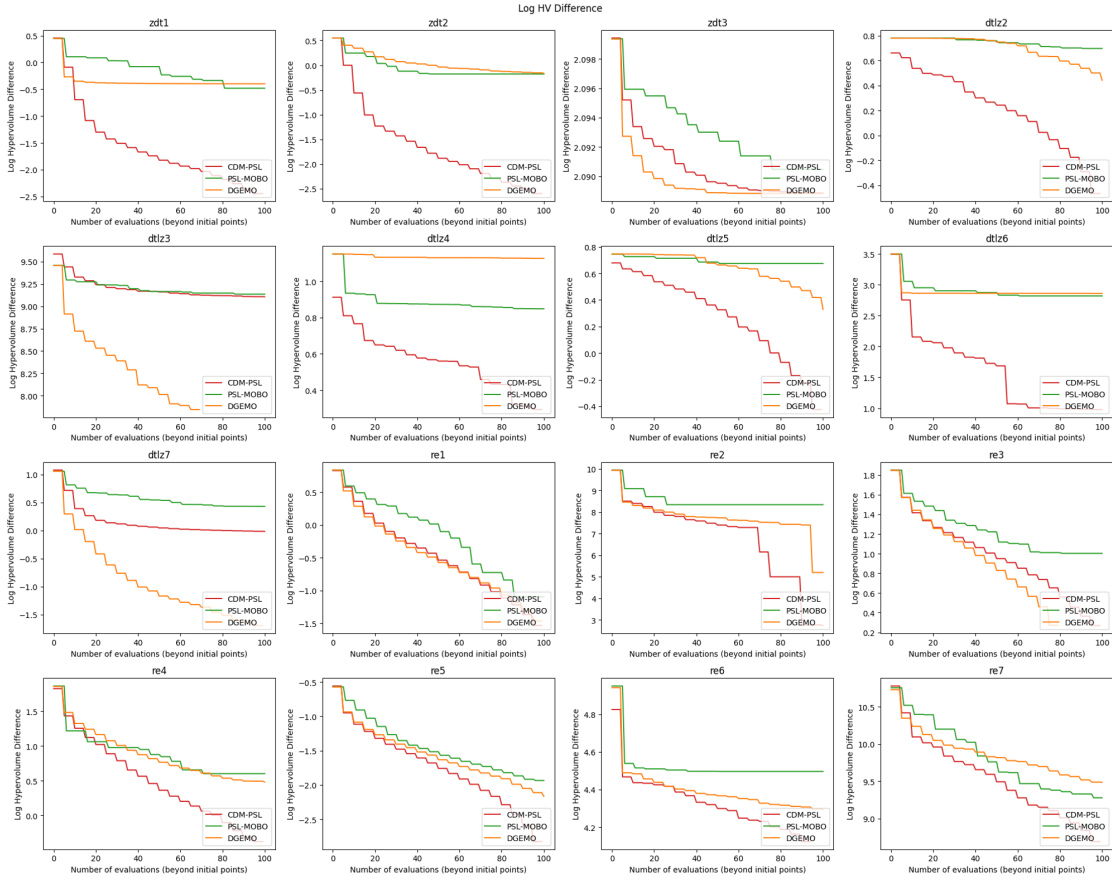


Figure 13. The log HV difference of 3 competitive algorithms, evaluated on synthetic test functions and real-world problems ($d = 20$).

Table 5. Time overhead of algorithm components in CDM-PSL.

Instance	Training		CG		UG		Other		CDM-PSL Time(s)	PSL-MOBO Time(s)
	Time(s)	Proportion	Time(s)	Proportion	Time(s)	Proportion	Time(s)	Proportion		
ZDT1 ($d = 10$)	12.5578	21.13%	9.5404	16.05%	1.7426	2.93%	35.5903	59.88%	59.4311	32.5015
ZDT1 ($d = 20$)	12.5281	22.11%	12.5824	22.20%	1.7389	3.07%	29.8183	52.62%	56.6677	38.7551
DTLZ2 ($d = 10$)	12.5111	14.32%	12.9713	14.85%	1.7146	1.96%	60.1494	68.86%	87.3464	55.2474
DTLZ2 ($d = 20$)	12.5622	13.33%	18.2628	19.38%	1.7364	1.84%	61.6794	65.45%	94.2408	58.8312

D. More Explanations About the Motivation of the Proposed Method

D.1. Motivation of using DM in PSL-based MOBO

When addressing EMOPs, the performance of PSL methods might deteriorate significantly due to the **complexity of distributions** of Pareto optimal solutions and the **limitation of function evaluations**. This poses a significant challenge to existing PSL algorithms (Lin et al., 2022). Unlike existing methods that directly learn the distribution of the PS in a single-step way, **complex distributions of solutions can be learned step by step with the aid of DM**. The success of DM in various domains (e.g. computer vision) shows promise for its application in PSL in EMOPs.

D.2. Detailed motivation

Using DM for MOBO is not trivial, because one should take into account the following two aspect: how to speed up the searching process and how to balance convergence and diversity. Having this in mind, we proposed a PSL method with composite diffusion models. Specifically, the proposed CDM-PSL has the following features:

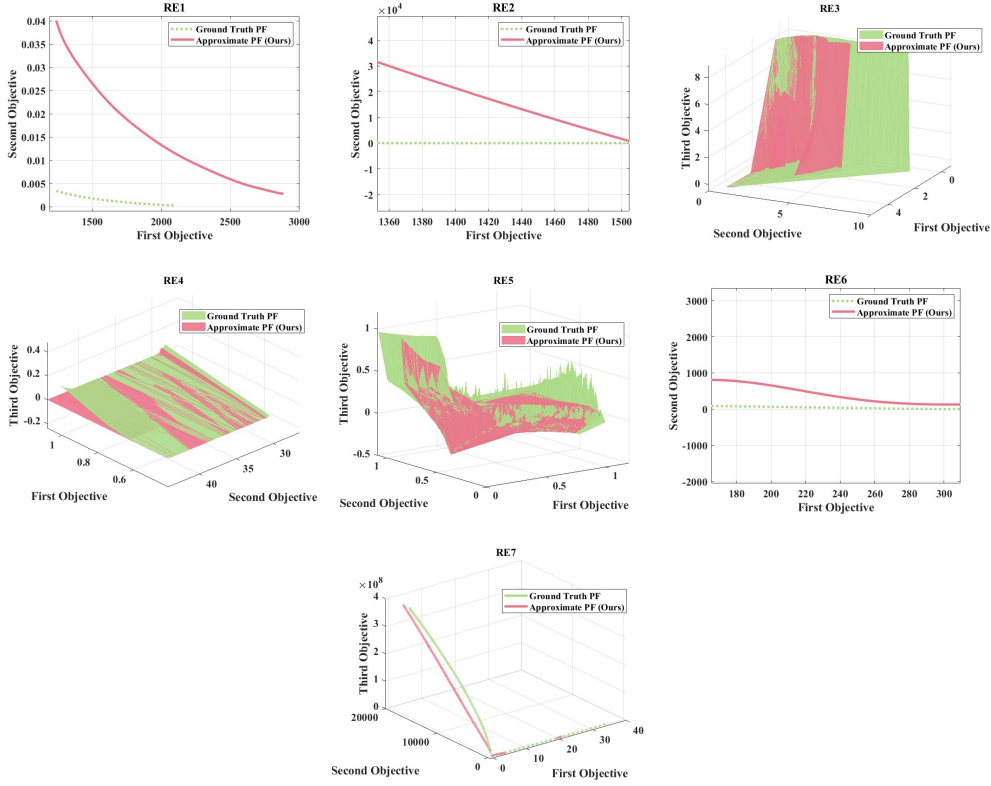


Figure 14. Approximate Pareto fronts obtained by CDM-PSL in real-word problems. ($d = 20$, $FE = 100$)

- CG with conditional DM is aimed at **better convergence** since it introduces gradient information to guide the searching process.
- UG with unconditional DM is designed for generating **diverse** solutions with low cpu-time cost.
- The entropy weighting method, serving as an objective aggregation approach for offering performance gradient information, is introduced to assign weights based on the information entropy of objectives. This method reduces subjectivity in weighting gradients for different objective values, and **ensures that the algorithm places more emphasis on objectives with rich information content**. Figure 7 shows that CG with entropy weighting method can generate better solutions than CG with mean weighting or random weighting.

E. Limitations of CDM-PSL

In this section, we will discuss some limitations of CDM-PSL. One limitation of our approach is that CG will introduce additional time overhead. As shown in Table 5, conditional generation increases the time overhead of generating candidate solutions to some extent, which leads to the limitations of the method in terms of excessive time overhead when applied to very high dimensional problems. Another limitation of our work is that our experiments were not conducted on real-world problems with very high dimensionality. While we have conducted experiments on seven real-world engine design problems, RE1-RE7, which can provide some evidence of the superiority of CDM-PSL in facing real-world problems, these test cases do not represent the complexity and scale of extremely high-dimensional industrial problems. We will explore the algorithm’s performance on super large problems like real industrial design in future work.

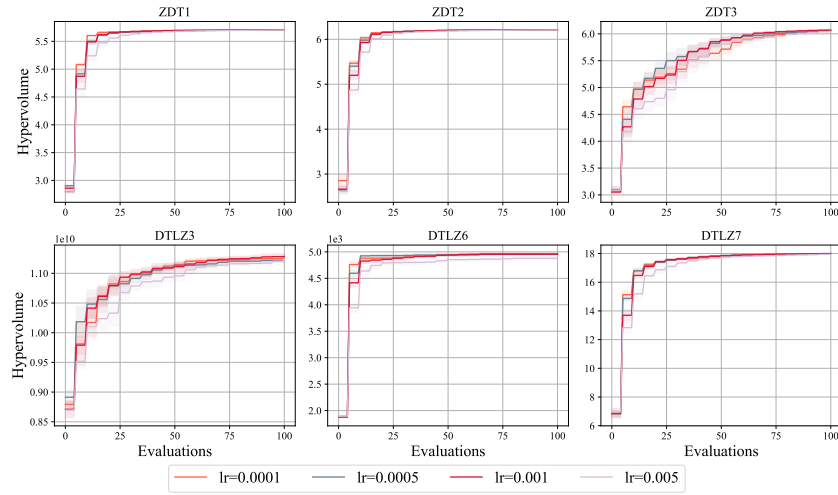


Figure 15. The HV results of CDM-PSL at different learning rate ($d = 20$).

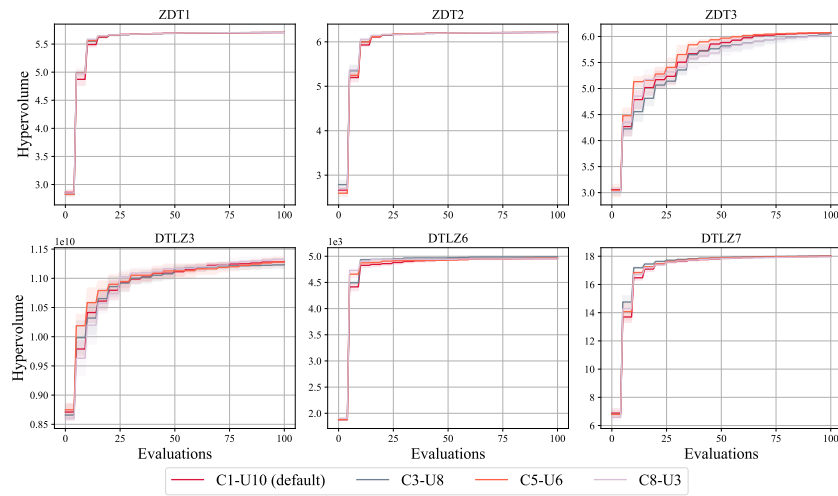


Figure 16. The HV results of CDM-PSL with different CG and UG ratios ($d = 20$).